

## Article

# Effect of Mullite Film Layers on the High-Temperature Oxidation Resistance of AISI 304 Stainless Steel

Jing Ma<sup>1,2,\*</sup> , Ning Wen<sup>1</sup>, Ruiyang Wang<sup>1</sup>, Jiangan Wang<sup>1,\*</sup>, Xin Zhang<sup>1</sup>, Jianhui Li<sup>1</sup> and Yiqing Chen<sup>3,\*</sup>

<sup>1</sup> School of Materials Science and Engineering, Hebei University of Science and Technology, Shijiazhuang 050018, China; wenning0619@163.com (N.W.); w15632310449@163.com (R.W.); zhixin5210@163.com (X.Z.); lijianhui\_97@163.com (J.L.)

<sup>2</sup> Hebei Key Laboratory of Material Near-Net Forming Technology, Shijiazhuang 050018, China

<sup>3</sup> State Key Laboratory of Metal Material for Marine Equipment and Application, Anshan 114009, China

\* Correspondence: majingt@hebust.edu.cn (J.M.); wm094212@163.com (J.W.); chenying2003@163.com (Y.C.)

**Abstract:** Protective coating is an effective way to extend materials' high-temperature service life. In order to improve the high-temperature oxidation resistance of AISI 304 stainless steel, mullite films with different layers were successfully prepared by the sol-gel method and the sintering process on the surface of stainless steel. The effect of the film layers on the high-temperature oxidation resistance of stainless steel at 900 °C for 100 h was studied. The analysis results of oxidation kinetics, X-rays diffraction (XRD), scanning electron microscopy (SEM) and energy dispersive analysis (EDS) show that  $Al_{1.4}Si_{0.3}O_{2.7}$  mullite film effectively improved the high-temperature oxidation resistance of stainless steel. The sample with three-layer mullite film has the best high-temperature oxidation resistance. The mass gain and oxidation spalling mass are only 4.6% and 34.5% of those of the uncoated sample after 100 h cyclic oxidation at 900 °C. A chromium oxide layer was formed at the interface of mullite film and the substrate during the sintering process. The generation of selective  $Cr_2O_3$  scale was promoted at the cyclic oxidation stage so that the sample with three-layers has excellent high-temperature oxidation resistance.

**Keywords:** sol-gel method; mullite film; film layers; high-temperature oxidation resistance; selective oxidation



**Citation:** Ma, J.; Wen, N.; Wang, R.; Wang, J.; Zhang, X.; Li, J.; Chen, Y. Effect of Mullite Film Layers on the High-Temperature Oxidation Resistance of AISI 304 Stainless Steel. *Coatings* **2021**, *11*, 880. <https://doi.org/10.3390/coatings11080880>

Academic Editor: Maria Vittoria Diamanti

Received: 23 June 2021

Accepted: 16 July 2021

Published: 23 July 2021

**Publisher's Note:** MDPI stays neutral with regard to jurisdictional claims in published maps and institutional affiliations.



**Copyright:** © 2021 by the authors. Licensee MDPI, Basel, Switzerland. This article is an open access article distributed under the terms and conditions of the Creative Commons Attribution (CC BY) license (<https://creativecommons.org/licenses/by/4.0/>).

## 1. Introduction

AISI 304 stainless steel is widely used in traditional industrial fields such as automobile manufacturing, power equipment, petrochemical industry, etc, by virtue of its excellent comprehensive mechanical properties, corrosion and high-temperature oxidation resistance [1–3]. High Cr, Ni and low carbon content make it keep austenite state and be applied in an environment below 800 °C. However, AISI 304 stainless steel will be oxidized at a faster rate when the temperature reaches 900 °C, which limits its application in a wider range [4–6]. The high-temperature oxidation rate of materials could be improved by means of alloy addition, micro-crystallization [7–9], pre-oxidation [10], reactive element addition [10] and protective coating/film [11–14], among which protective coating/film is an effective way to extend materials' service life.

There are many processes for preparing high-temperature protective coating/film. Compared with other coating technology, the sol-gel reaction precursor is uniformly dispersed in the solution and the reaction proceeds at the molecular level. Therefore, a highly pure and uniform film can be obtained by the sol-gel method [15–20]. Mullite is a ceramic material composed of  $Al_2O_3$  and  $SiO_2$ , which has the characteristics of low expansion coefficient, high melting point, strong corrosion resistance and excellent thermal shock resistance [21–25]. It is a potential high-temperature engineering material [26–30] due to its excellent high-temperature performance, which makes it widely used in kiln linings, pipelines, and steam turbines. Different kinds of mullite materials are prepared

and used for the water vapor corrosion at elevated temperature [29], hot gas and oily water cleaning and antibacterial biofilm.

Mullite film/coating is used to improve high-temperature oxidation of C/C composites [30–32] and stainless steel [33]. Lei Zhou prepared mullite whisker-mullite/yttrium aluminosilicate coating on SiC coated C/C composites. The porous mullite middle coating prepared by supersonic atmospheric plasma spraying relieves the concentration of stress, improving thermal shock properties and oxidation resistance at 1773 K [30]. Pengju Chen deposits a novel tri-layer  $\text{Yb}_2\text{Si}_2\text{O}_7/\text{Al}_6\text{Si}_2\text{O}_{13}/\text{SiC}$  environment barrier coatings (EBCs) on the surface of Cf/SiC composites. The mullite middle coating prepared by the air spray sol-gel method can efficiently prevent the oxidation of Cf/SiC composites at 1673 K [31]. Wen successfully prepared a dense and uniform mullite coating on the carbon/carbon composite material by the sol-gel method. The coating provides effective high-temperature protection for the carbon/carbon composite material [32]. Ma H prepared mullite coatings were prepared on stainless steel by the sol-gel and dip-coating method. The influences of sol concentration, heating time, heating rate, sintering temperature on the quality of the mullite coatings were studied. The optimum sintering temperature was obtained through the thermal shock resistance test [33]. However, few reports have been found on the effect of mullite film layers on the high-temperature oxidation resistance of stainless steel. In this paper, a sol-gel method was used to prepare mullite film on the surface of 304 stainless steel, and the effect of mullite film and the number of film layers on the high-temperature oxidation resistance of AISI 304 stainless steel and the corresponding mechanism was studied.

## 2. Materials and Methods

### 2.1. Substrate Pretreatment

The rolled AISI 304 stainless steel plate was used as substrate. Its chemical composition and mechanical property are shown in Tables 1 and 2. It was cut into a square sample (15 mm × 15 mm × 3.5 mm) with an SXC-73 type wire cutting device produced by Jiangxi Wuji Shiye Co., Ltd. (Nanchang, China). The samples were ground with 200, 400, 600 and 800 sandpaper to remove the surface oxide layer. The ground stainless steel samples were placed in a KH-50B ultrasonic instrument produced by Kunshan Hechuang Ultrasonic Instrument Co., Ltd. (Kunshan, China), washed with deionized water and absolute ethanol for 5 min respectively, and then dried in an HY-RH30-500 drying oven produced by Dongwan Hongjin Testing Instrument Co. Ltd. (Dongguan, China) for later use.

**Table 1.** Chemical composition of AISI 304 stainless steel.

Element	Cr	Ni	C	Si	Mn	Cu	V	Fe
Content/wt.%	18.24	7.90	0.065	0.42	1.25	0.019	0.60	Bal.

**Table 2.** Mechanical property of AISI 304 stainless steel.

Property	$\sigma_b$	$\sigma_{0.2}$	$\delta_5$	$\psi$	HRC
Value	≥520 MPa	≥205 MPa	≥40%	≥60%	29.8

### 2.2. Preparation of Mullite Precursor Sol

Tetraethyl orthosilicate (TEOS) was dissolved in ethanol at room temperature, stirred for 30 min to uniform mixing and then heated to 60 °C. Deionized water and nitric acid were added. The pH of the solution was adjusted to 2 with  $\text{HNO}_3$ . The solution was stirred for 60 min until the color turns to translucent, then aged at room temperature for 6 h to obtain a transparent  $\text{SiO}_2$  sol. Aluminum isopropoxide ( $[(\text{CH}_3)_2\text{CHO}]_3\text{Al}$ ) was dissolved in excess deionized water at 90 °C, closed stirred for 1.5 h and then open stirred for 30 min to obtain the hydrolyzed boehmite. Meanwhile, the isopropanol produced by hydrolysis was volatilized. Deionized water was added in time to ensure the final molar ratio of aluminum

isopropoxide to deionized water is 1:100. The  $\text{HNO}_3$  peptizer was added to adjust the sol's pH to 2 and closed stirred for 1 h. The clear  $\text{Al}_2\text{O}_3$  sol was obtained by refluxed and aged for 12 h at 90 °C. The prepared  $\text{SiO}_2$  sol was added dropwise to the  $\text{Al}_2\text{O}_3$  sol until the molar ratio of Si to Al is 1:3.  $\text{HNO}_3$  was added dropwise to adjust the pH to 2. The mixing sol was then stirred for 1 h.  $\text{B}_2\text{O}_3$  flux was added to sol solution where the mass ratio of  $\text{B}_2\text{O}_3$  to mullite is 1:2. Mullite film precursor sol was obtained after stirred for 1 h.

### 2.3. Preparation of Mullite Film

The pretreated sample was dipped in mullite sol for 60 s and then pulled at a speed of 10 mm/min by a YYF-50 slow strain rate stress testing machine produced by Shanghai Bairuo Testing Instrument Co., Ltd. (Shanghai, China) After each dipping operation, the sample was dried at room temperature for 20 min and then placed in an HY-RH30-500 drying oven at 100 °C for 20 min to complete an operation. According to the above method, samples with one, three, six, and nine film layers were prepared respectively. The sintering process was carried out in a GSL-1500X type vacuum tube furnace produced by Hefei Kejing Material Technology Co., Ltd. (Hefei, China) The samples were heated to 300 °C at a heating rate of 5 °C/min and held for 20 min, then heated at 5 °C/min to 900 °C and held for 60 min, and finally furnace cooled to room temperature. The mullite films with different layers were obtained. Argon gas of 5N with a flow rate of 0.1 L/min was used as protective gas during the sintering process.

### 2.4. Oxidation Tests

The cyclic oxidation method was used to characterize the high-temperature oxidation resistance of the samples. The samples were put into crucibles to collect the spallation scales. After measuring the surface areas of the samples, the crucibles with samples were put in an SRJX-4-13 muffle furnace produced by Tianjin Taist Instrument Co., Ltd. (Tianjin, China) at 900 °C for 100 h. The crucibles with and without samples were weighed in an FA2004N electronic balance with an accuracy of  $10^{-5}$  g produced by Shanghai Precision Scientific Instrument Co., Ltd. (Shanghai, China) after being air cooled for 20 min for each 10 h exposure. Oxidation kinetics curves were plotted by the mass gain and spallation mass of the samples vs. time. Before oxidation, the crucibles were heated to 900 °C for 10 h to remove the moisture and other high-temperature volatile substances so as to minimise experimental error.

### 2.5. Analysis Method

The samples coated with different layers before and after cyclic oxidation were set by XQ-2Bφ22 metallographic specimen mosaic machine produced by Laizhou Weiyi Test Instrument Manufacturing Co., Ltd. (Yantai, China) Their cross sections were ground with SiC sandpaper and finally polished. The surface and cross section morphology of the filmed samples were observed by TESCAN VEGA3 SEM (Brno, Czech Republic), and the composition and phases were analyzed by Oxford x-stream-2 EDS (Abingdon, UK) and RIGAKU D/MK2 500 XRD (Tokyo, Japan).

## 3. Results and Analysis

### 3.1. Morphology and Composition of Mullite Film

Figure 1 shows the SEM surface morphology of the AISI 304 stainless steel coated with different mullite layers. For single-layer and three-layer mullite film samples (Figure 1a,b), the ground marks can be clearly observed, which indicates the thicknesses of films were relatively thin. Many tiny particles were present on the surface. For the single-layer mullite film sample, the film was imperfect and noncontinuous, shown as point A. For the six-layer mullite film sample (Figure 1c), the ground marks can be vaguely seen, indicating that the mullite film was thicker. There were many small cracks, whose width was about 1~2 μm. Traces of film spalling can be seen, shown as point B. For the nine-layer mullite film sample (Figure 1d), the film was the thickest. There were more large cracks, the width of which

was about 2~4  $\mu\text{m}$ . So the three-layer film was more closely bonded to the stainless steel and continuous.

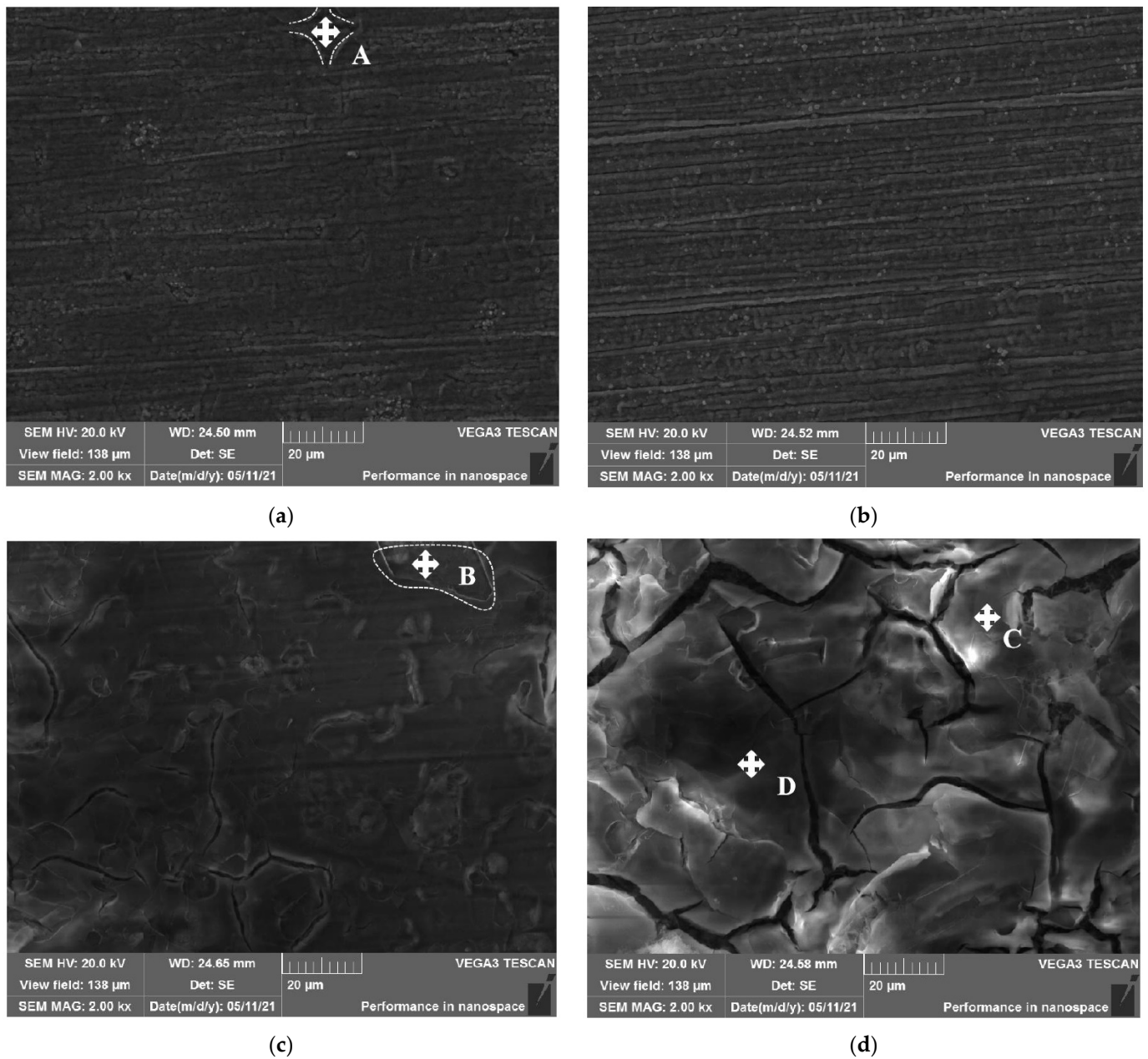


**Figure 1.** SEM surface morphology of mullite films after sintering with different layers: (a) single-layer; (b) three-layer; (c) six-layer; (d) nine-layer.

EDS analysis of the points C and D in Figure 1d are shown in Table 3. The black gray oxide layer on the surface was mainly composed of Al and Si oxides. The measured molar ratio of Al:Si was about 3:1, which was consistent with the element ratio in mullite sol, indicating that mullite had been successfully prepared on the surface of stainless steel, and the film composition was uniform. Fe and Cr elements can be also found.

**Table 3.** EDS analysis results at the mark of the sample coated with nine-layer of mullite film.

Symbol	At.%Fe	At.%Cr	At.%Al	At.%Si	At.%O	At.%Ni
C	10.26	4.59	23.16	7.27	53.73	1.00
D	16.81	5.99	16.89	4.93	53.64	1.74

Figure 2 is the cross section morphology of samples with different layers of films after sintering. The film was very thin. It is difficult to determine its thickness. EDS element line scan for samples with nine-layer film shows that the film was about 2  $\mu\text{m}$  due to the high content of Al, Si and O. A diffusion layer of about 1  $\mu\text{m}$  was formed, which was rich in Cr and O. It is speculated to be  $\text{Cr}_2\text{O}_3$ . For a film with fewer layers, its thickness may be nano-scale. Meanwhile, the thickness of the film was not uniform.

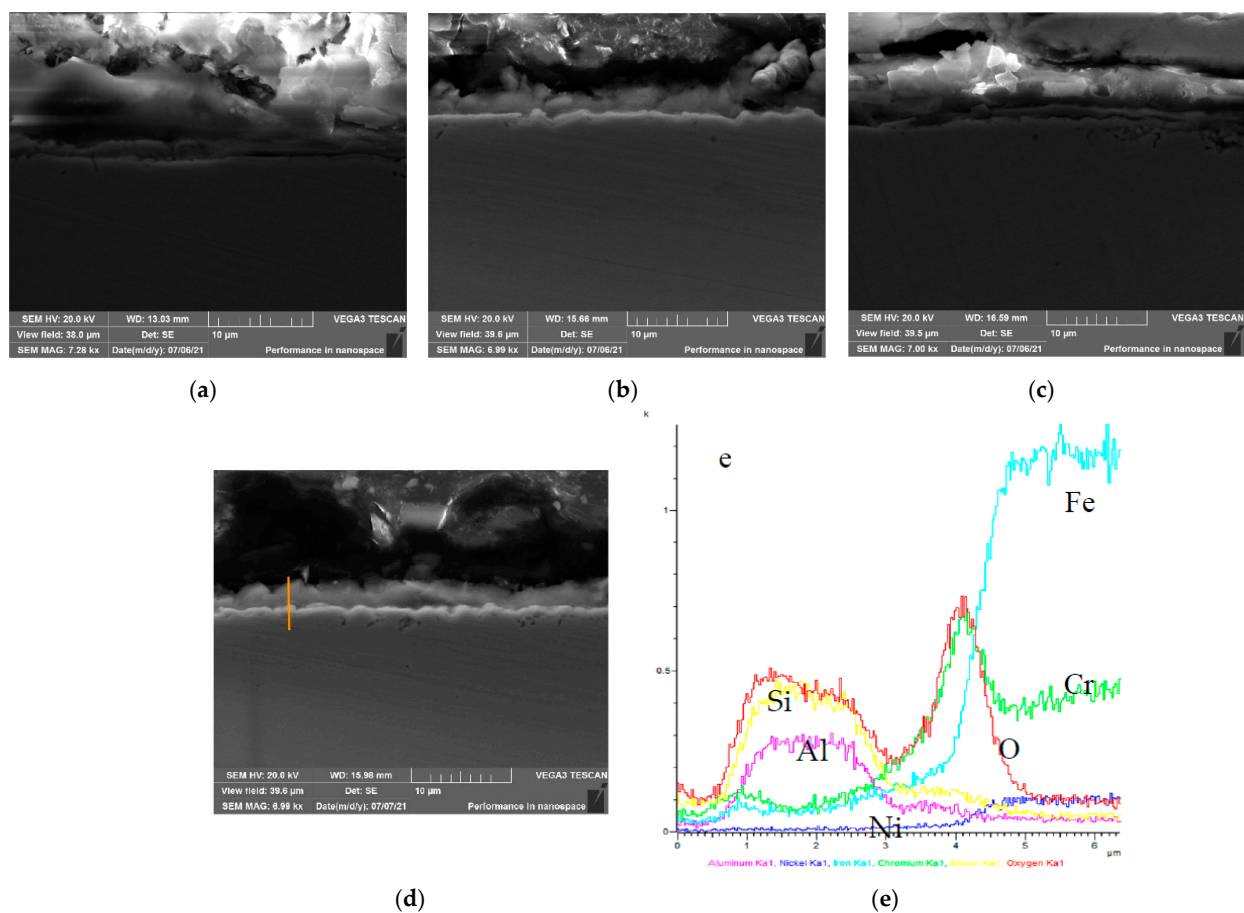


**Figure 2.** Cross section morphology and EDS of mullite film samples with different layers after sintering: (a) single-layer; (b) three-layer; (c) six-layer; (d) nine-layer; (e) EDS line scan of the yellow line in (d).

### 3.2. Oxidation Kinetics Analysis

Figure 3 shows the oxidation kinetics curves of the samples uncoated and coated with mullite film of different layers cyclically oxidized in air at 900  $^{\circ}\text{C}$  for 100 h. The oxide mass gain and the spallation mass of the uncoated sample were the largest, which were 0.65 and 0.44  $\text{mg}/\text{cm}^2$  respectively. After 100 h cyclic oxidation, the oxide mass gain curve of the uncoated sample showed an almost linear growth trend in the first 70 h, and the oxide mass gain at the last oxidation stage (70–100 h) increased slowly. Compared with that of uncoated, the high-temperature oxidation resistance of the samples coated with different mullite layers film had been improved obviously. The oxide mass gain of mullite film decreased with the increase of the number of film layers while the oxide spallation mass

increased with the increase of the number of film layers. The oxide mass gain of single, three, six and nine layer samples were 0.36, 0.15, 0.14 and 0.03  $\text{mg}/\text{cm}^2$ , respectively, which were 55.4%, 23.1%, 21.5% and 4.6% of the uncoated sample. The oxide spallation mass of single, three, six and nine layer samples were 0.05, 0.05, 0.09 and 0.15  $\text{mg}/\text{cm}^2$ , which were 11.3%, 11.3%, 20.5% and 34.1% of the uncoated sample. The sample coated with three-layer mullite film has the best high-temperature resistance.

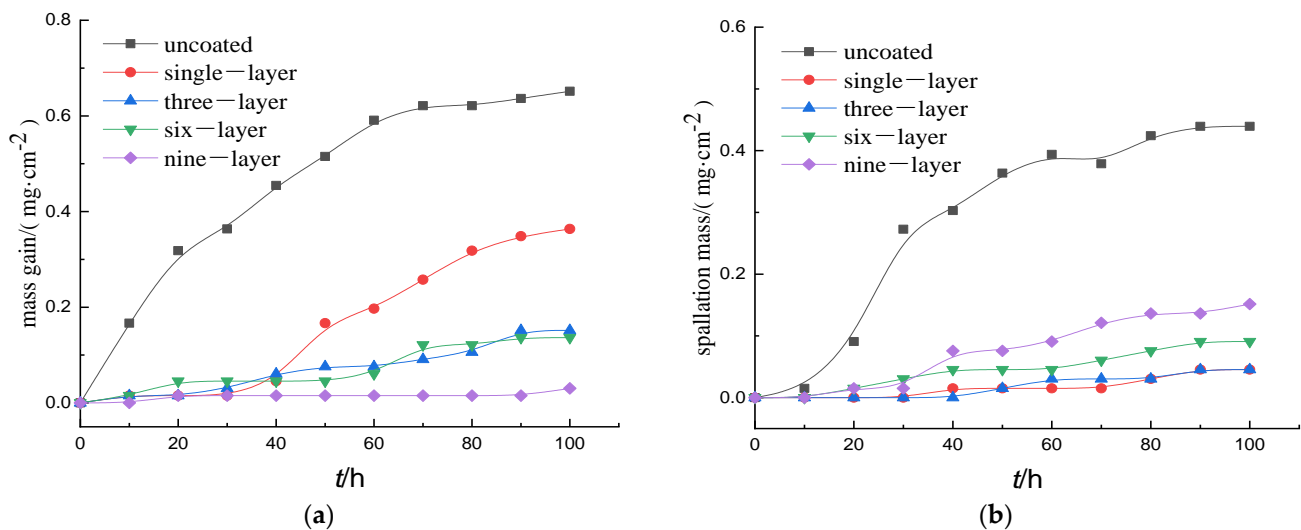


**Figure 3.** Oxidation kinetics curve of uncoated sample and mullite film samples with different layers at 900 °C in air: (a) mass gain; (b) spallation mass.

### 3.3. Surface Morphology and Phase Analysis of Oxide Scale Layer

Figure 4 and Table 4 show the SEM surface morphology and EDS analysis of 304 stainless steel uncoated and coated with different mullite layers film oxidized at 900 °C for 100 h. The surface of the uncoated sample (Figure 4a) was loose and porous, with obvious cracking marks. The surface of the sample coated with single-layer mullite film (Figure 4b) was completely covered by newly formed oxides, the oxide distribution was relatively uniform, and slight cracks were present on the surface. The prepared film was not visible. For the samples with three-layer, six-layer and nine-layer films, granular particles with regular geometric shapes were growing out at the cracks of the large pieces of the film. The composition (point F) was mainly Cr and O, which means it was the  $\text{Cr}_2\text{O}_3$  phase. The composition of the flat film (point E) was mainly Al, Si and O, which shows that mullite film still existed after 100 h oxidation at 900 °C and gave effective protection to the stainless steel substrate. The cracks on the surface of samples with six-layer and nine-layer film were wide. Some oxide particles were loosely present on films. The EDS results of the oxides scale show that the contents of Al, Si and O elements increase with the increase of layers, which indicates the thicker film for more layers. The ratio of Cr/Fe of the oxides scale for the uncoated sample was 16.74, which was higher. The Cr/Fe ratio decreases with the increase of the layer number.

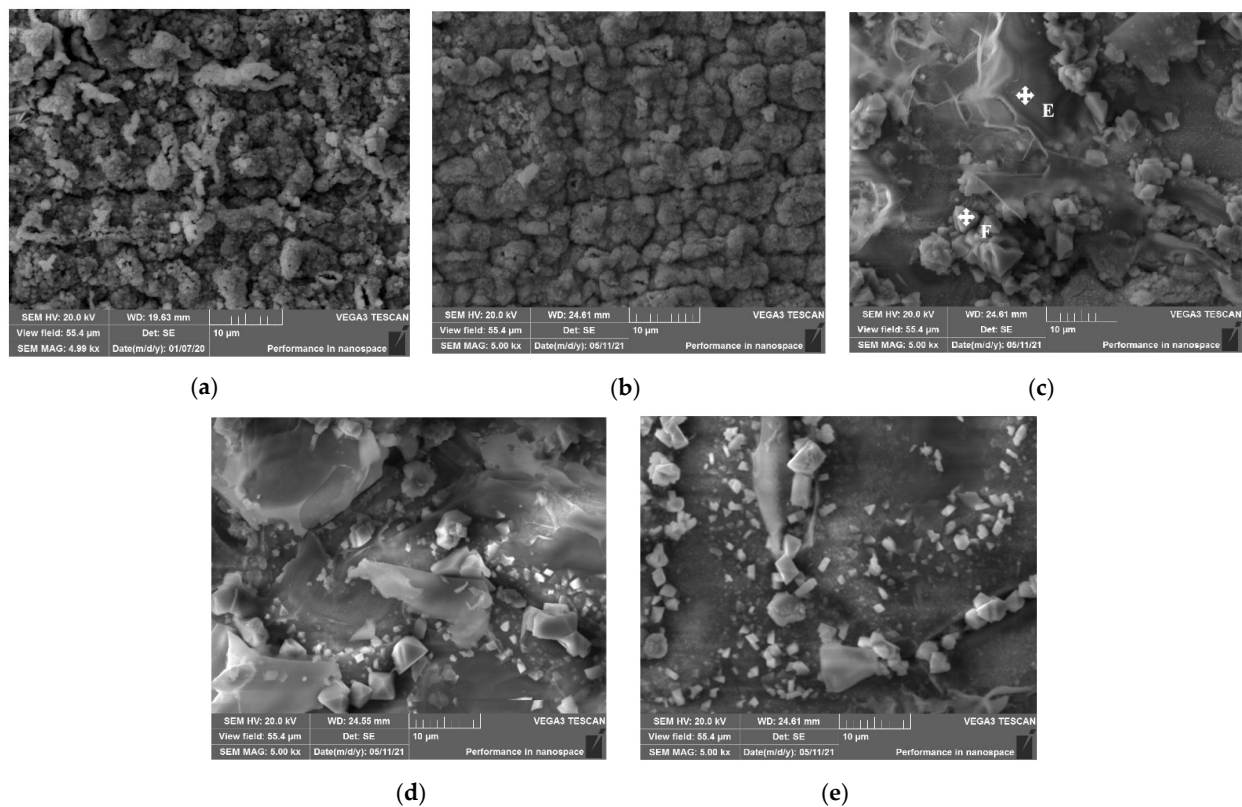
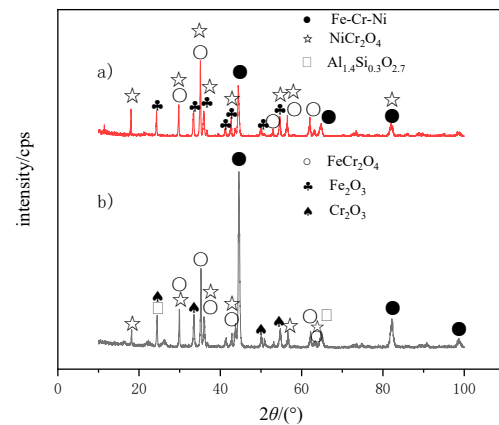


**Figure 4.** SEM surface morphology of samples uncoated and coated with different layers of mullite film after cyclic oxidation at 900 °C for 100 h: (a) uncoated; (b) single-layer; (c) three-layer; (d) six-layer; (e) nine-layer.

**Table 4.** EDS analysis results of the sample with different-layer of mullite film after oxidation.

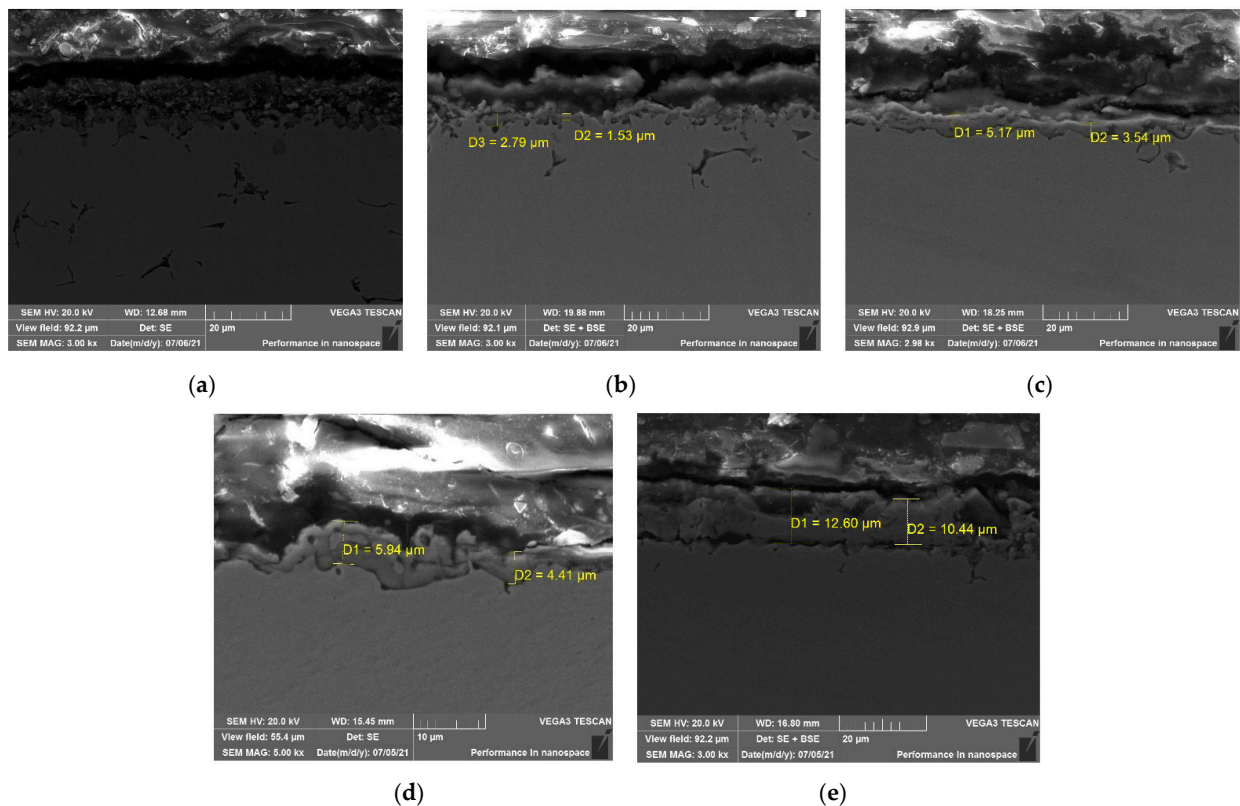
Site	Wt.%Fe	Wt.%Cr	Wt.%Al	Wt.%Si	Wt.%O	Wt.%Ni	Cr/Fe Ratio
Uncoated	3.61	60.42	-	-	35.55	0.42	16.74
Single layer	2.78	59.08	0.32	0.34	37.23	0.25	21.25
Three-layer	3.99	53.50	3.22	1.16	37.69	0.44	13.41
Six-layer	5.34	45.68	7.38	2.54	38.58	0.47	8.55
Nine-layer	6.49	35.79	11.82	3.94	41.45	0.51	5.51
Point E	1.03	16.12	25.84	8.19	48.82	-	-
Point F	1.09	46.74	0.74	0.11	51.23	0.09	-

Figure 5 shows the XRD spectra of the samples uncoated and coated with a nine-layer mullite film after cyclic oxidation at 900 °C for 100 h. It can be seen that the oxides scales of the uncoated sample are mainly composed of  $\text{Fe}_2\text{O}_3$ ,  $\text{NiCr}_2\text{O}_4$ ,  $\text{FeCr}_2\text{O}_4$  while  $\text{Al}_{1.4}\text{Si}_{0.3}\text{O}_{2.7}$  mullite film phase and  $\text{Cr}_2\text{O}_3$  with excellent high-temperature oxidation resistance can also be found on the surface of the film sample. For both cases, the substrate peak of Fe-Cr-Ni phase can be detected. The higher peak of Fe-Cr-Ni phase and the formation of selective  $\text{Cr}_2\text{O}_3$  oxide phase for the film sample indicate that its oxides scale was thinner and excellent protective.



**Figure 5.** XRD spectra of sample uncoated and coated with nine-layer mullite film after cyclic oxidation at 900 °C for 100 h: (a) uncoated sample; (b) coated nine-layer mullite film sample.

Figure 6 shows the cross section morphology of the samples uncoated and coated with different-layer films after oxidation. The oxides scale formed on the uncoated sample were thicker and had a lamellar structure. Many cracks were present. A few internal oxides were formed for the sample with a single layer, indicating its poor protection. A continuous thin oxide scale layer was formed on the samples with three-layer and six-layer film, whose thickness was very close. A relatively thicker oxides scale layer was formed for the sample with nine-layer, which means that the complex scale phases were present. It is consistent with the XRD results.



**Figure 6.** SEM cross section morphology of mullite films after sintering with different layers: (a) uncoated; (b) single-layer; (c) three-layer; (d) six-layer; (e) nine-layer.

Figure 7 is the EDS line scanning analysis of a sample with three layers. There are two peaks of Si element on the outmost layer. The width of Si peak was about 3 μm. The

content of Cr and O was high between the film and the substrate. A protective chromium oxide layer about 6  $\mu\text{m}$  thickness was formed on the surface of the substrate. The Al content was high in all layers, indicating that the Al element diffused into the oxide layer.

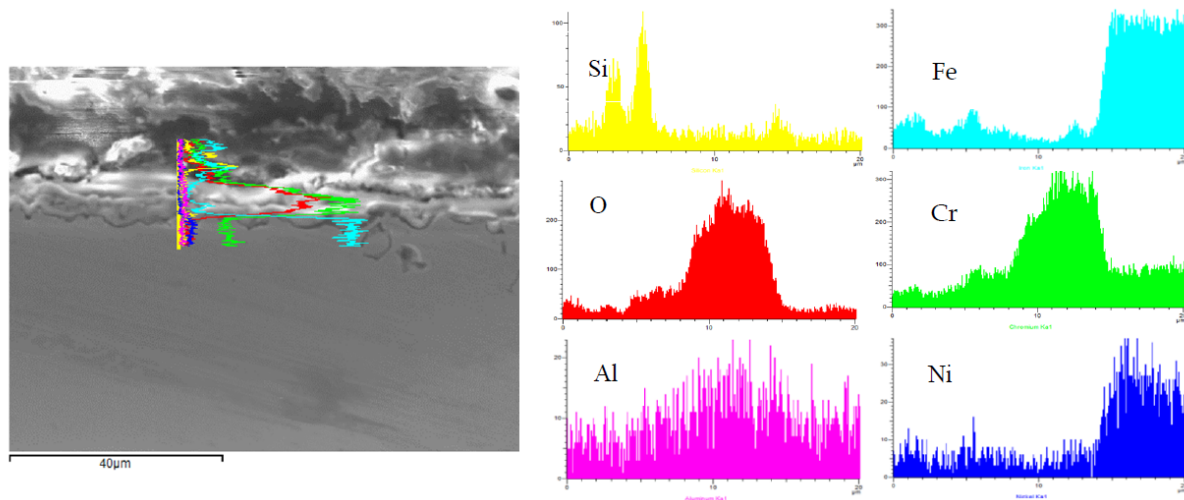


**Figure 7.** EDS line scanning analysis of stainless steel coated mullite films with three layers after cyclic oxidation.

#### 4. Analysis and Discussion

It is well known that  $\text{Cr}_2\text{O}_3$ ,  $\text{Al}_2\text{O}_3$  and  $\text{SiO}_2$  protective oxide scales can effectively improve the high-temperature oxidation of materials. Mullite is a refractory aluminosilicate with high thermal stability, whose molecular stoichiometry is normally between  $3\text{Al}_2\text{O}_3 \cdot 2\text{SiO}_2$  and  $2\text{Al}_2\text{O}_3 \cdot \text{SiO}_2$  [24]. In our study,  $\text{Al}_{1.4}\text{Si}_{0.3}\text{O}_{2.7}$  mullite film was formed, which can be written as  $7\text{Al}_2\text{O}_3 \cdot 3\text{SiO}_2$ . The higher the ratio of alumina to silica, the higher the melting temperature of mullite so that the high-temperature oxidation resistance is better [24]. Strictly speaking, the film is not a real mullite film. Yet  $\text{Al}_{1.4}\text{Si}_{0.3}\text{O}_{2.7}$  mullite film has excellent performance. The addition of  $\text{B}_2\text{O}_3$  flux can remarkably decrease the formation temperature of mullite [30], which is very important to stainless steel for too high heating temperature will weaken the steel.

Mullite has an orthorhombic crystal structure. It is composed of  $\text{AlO}_6$  octahedron along the *c*-axis, co-top cross-linked with  $\text{SiO}_4$  tetrahedron and  $\text{AlO}_4$  tetrahedron. Its crystal structure provides it stable chemical properties. Mullite's thermal conductivity (3.83 W/m·K at 1000 °C) [23] is one magnitude lower than those of  $\text{Al}_2\text{O}_3$  (20–32 W/m·K) and  $\text{SiO}_2$  (27 W/m·K), which can effectively block heat transfer to the substrate steel. Moreover, mullite would not have allotropic transformation during heating and cooling, which avoids the volume mutation during the heat treatment process of application.

The high-temperature oxidation performance of the film is not only related to the film's nature but also affected by the continuity. To improve the protective effect of the film, the thicker film is desired regardless of the economy. However, too thick a film may lead to excessive stress in the film. The film's volume would change during the sintering process. The reaction formula of mullite formation can be expressed as:



It is assumed that the densities of the  $3\text{Al}_2\text{O}_3 \cdot 2\text{SiO}_2$  and  $7\text{Al}_2\text{O}_3 \cdot 3\text{SiO}_2$  are the same, which is 3.2 g/cm<sup>3</sup>. The densities of  $\text{Al}_2\text{O}_3$  and  $\text{SiO}_2$  are 3.5 g/cm<sup>3</sup> and 2.2 g/cm<sup>3</sup> respectively. According to the molar weight and density of reactants and resultants, the volume shrinkage of  $3\text{Al}_2\text{O}_3 \cdot 2\text{SiO}_2$  is 93.9% while that of  $7\text{Al}_2\text{O}_3 \cdot 3\text{SiO}_2$  is 97.8%. So the residual stress in mullite film is tensile stress. When the film layer is thin, the stress in the film can

be released. With the increase of film layers, the stress in film increases. When the stress exceeds the strength of the film, cracking occurs. So many cracks were generated on the mullite film with excessive thick nine-layer. The stress in mullite film with moderate layers (three layers) is lower so that the film is continuous and well bonded to the substrate.

Although mullite has excellent high-temperature performance, the thermal properties of film and substrate are quite different. The thermal expansion coefficient of mullite film ( $5.6 \times 10^{-6}/\text{K}$ ) [34] is quite different from that of 304 stainless steel substrate ( $18\text{--}20 \times 10^{-6}/\text{K}$ ) [35]. The mismatch of the thermal expansion coefficient during the cyclic oxidation process would cause the increase of internal stress in film, which will reduce the bonding strength and generate defects such as cracks and peeling. For the high temperature oxidation process of coated metal samples, the oxidation reaction is mainly controlled by the mutual diffusion of oxygen inward and base metal elements outward through the film. Thus, the property and the layer numbers of mullite film will greatly influence the oxidation process.

At cyclic oxidation temperature of  $900\text{ }^\circ\text{C}$ , the oxygen activity is stronger [36]. For the uncoated sample, the metal elements on the surface of the substrate and oxygen can directly react at a relatively rapid rate so that the oxide scale is loose and porous.  $\text{Fe}_2\text{O}_3$  with poor protection is generated besides  $\text{NiCr}_2\text{O}_4$  and  $\text{FeCr}_2\text{O}_4$ , which cannot provide effective protection to the substrate. The spallation mass is the highest. It is the spallation of  $\text{Fe}_2\text{O}_3$  oxide that leads to the higher Cr/Fe ratio of the oxides scale.

304 stainless steel coated with three-layer mullite film has the best high-temperature oxidation resistance. The reasons are as follows:

(1) The stress in three-layer mullite film is lower so that the prepared mullite film is well bonded and continuous. The presence of continuous film lowers the oxygen partial pressure on the surface of the substrate at the initial oxidation stage. According to Wagner's selective oxidation transition theory [37]:

$$N_B^{\min} > \frac{\sqrt{\pi} V_{AB}}{V_{BO}} \sqrt{\frac{k_p(P_{O_2})}{2D_B}} \quad (3)$$

where  $N_B^{\min}$  is the minimum content of the solute element (B) for selective oxidation;  $V_{AB}$  and  $V_{BO}$  are the molar volume of the alloy and BO respectively;  $D$  is the diffusion coefficient of B in the alloy;  $k_p(P_{O_2})$  is the parabolic velocity constant when BO is generated on pure B, which is the function of oxygen partial pressure.

For the oxidation of stainless steel, Cr and  $\text{Cr}_2\text{O}_3$  are solute elements B and BO respectively. If the oxygen partial pressure  $P_{O_2}$  on the surface of the steel is decreased, the parabolic velocity constant of  $\text{Cr}_2\text{O}_3$  oxide will be decreased. So the minimum content of the solute element (Cr)  $N_B^{\min}$  for selective oxidation will be decreased. The low oxygen pressure promotes the formation of the protective chromium oxide layer during the following cyclic oxidation process. Continuous selective  $\text{Cr}_2\text{O}_3$  scale with excellent high-temperature protection will be promoted (Figure 7). The  $\text{Cr}_2\text{O}_3$  phase in the XRD result of the sample with nine layers after oxidation (Figure 5) could verify the above point.

(2) Mullite film itself has outstanding high-temperature oxidation resistance. Its thermal conductivity is much lower, which can effectively decrease the surface temperature of AISI 304 stainless steel substrate. The decrease of service temperature will also improve the high-temperature oxidation performance. Furthermore, mullite's high melting temperature (about  $1850\text{ }^\circ\text{C}$ ) and stable chemical crystal structure are very important. Thus the high-temperature resistance of three-layer mullite film is excellent.

More details about the oxidation kinetics should be concerned. The mass gain of samples decreases with the increase of layer number. Yet the mass gain (Figure 3a) of samples with three and six layers are close. The film with six-layer is a little thicker than that with three-layer. However, there are some small cracks and peels in the six-layer film. The defects accelerate the oxidation process so that the mass gain is increased. The oxide scale layer after oxidation is similar. This may be the reason for their equivalent

mass gain. The spallation mass of samples increases with the increase of layer numbers (Figure 3b). The unreacted  $\text{Al}_2\text{O}_3$  and  $\text{SiO}_2$  during the sintering process would peel off from the surface of the film, which causes the degradation of spallation property. The one-layer and three-layer films have a similar surface morphology. The spallation mass of samples with one-layer and three-layer films is relatively low and close.

## 5. Conclusions

1.  $\text{Al}_{1.4}\text{Si}_{0.3}\text{O}_{2.7}$  mullite films of different layers were successfully prepared by the sol-gel method and sintering process on the surface of AISI 304 stainless steel. The high-temperature oxidation resistance of stainless steel samples with films was obviously improved. The results are consistent with the previous references.
2. The sample with three-layer mullite film has the best high-temperature oxidation resistance. The oxide mass gain and oxidation spalling mass are only 4.6% and 34.5% of those of the uncoated sample after cyclic oxidation at 900 °C for 100 h. A chromium oxide layer formed during the sintering process promotes the formation of selective  $\text{Cr}_2\text{O}_3$  scale with excellent high-temperature resistance.
3. Further research should be concerned about the sol-gel and sintering process, including the sol-gel formulation, sintering temperature and time.

**Author Contributions:** Conceptualization, J.M., J.W. and X.Z.; methodology, J.M., N.W. and R.W.; software, J.M. and N.W.; validation, J.M. and R.W.; formal analysis, J.M., N.W. and R.W.; investigation, J.M., N.W. and R.W.; resources, J.L. and Y.C.; data curation, J.M., N.W. and R.W.; writing—original draft preparation, J.M. and N.W.; writing—review and editing, J.W., X.Z. and J.L.; visualization, J.M.; supervision, J.W. and Y.C.; project administration, X.Z. and Y.C.; funding acquisition, J.M. and J.L. All authors have read and agreed to the published version of the manuscript.

**Funding:** This research was funded by the National Natural Science Foundation of China (Nos. 51761030 and 51701064), and open fund of State Key Laboratory of Metal Material for Marine Equipment and Application (No. SKLMEA-K202004).

**Institutional Review Board Statement:** Not applicable.

**Informed Consent Statement:** Not applicable.

**Data Availability Statement:** Data is contained within the article.

**Conflicts of Interest:** The authors declare no conflict of interest.

## References

1. Qiu, J.H. Passivity and its breakdown on stainless steels and alloys. *Surf. Interfaces Anal.* **2002**, *33*, 830–833. [[CrossRef](#)]
2. Martins, C.M.B.; Moreira, J.L.; Martins, J.I. Corrosion in water supply pipe stainless steel 304 and a supply line of helium in stainless steel 316. *Eng. Fail. Anal.* **2014**, *39*, 65–71. [[CrossRef](#)]
3. Zhang, H.; Li, Q.; Wang, Y.; Addae, M.; Jibrin, B.T.; Yang, J. Mechanical properties of zinc-aluminum film on steel cable substrate in corrosion environment. *J. Constr. Steel. Res.* **2018**, *150*, 288–297. [[CrossRef](#)]
4. Wang, S.G.; Sun, M.; Han, H.B.; Long, K.; Zhang, Z.D. The high-temperature oxidation of bulk nanocrystalline 304 stainless steel in air. *Corros. Sci.* **2013**, *72*, 64–72. [[CrossRef](#)]
5. Riffard, F.; Buscail, H.; Caudron, E.; Cuffe, R.; Issartel, C.; Perrier, S. The influence of implanted yttrium on the cyclic oxidation behaviour of 304 stainless steel. *Appl. Surf. Sci.* **2006**, *252*, 3697–3706. [[CrossRef](#)]
6. Issartel, C.; Buscail, H.; Caudron, E.; Cuffe, R.; Riffard, F.; Messki, S.E.; Perrier, S.; Jacquet, P.; Lambertin, M. Nitridation effect on the oxidation of a austenitic stainless steel AISI 304 at 900 °C. *Appl. Surf. Sci.* **2004**, *225*, 14–20. [[CrossRef](#)]
7. Ma, J.; He, Y.D.; Gao, W.; Wang, J.; Sun, B.D. The effect of micro-crystallizing on the oxidation resistance of Cu–Cr alloy in air. *Mater. Sci. Eng. A* **2008**, *488*, 311–317. [[CrossRef](#)]
8. Ma, J.; He, Y.D.; Sun, B.D.; Wang, J. The oxidation of micro-crystalline Co–Cr alloys under balanced oxygen pressure of  $\text{Co}_2\text{O}_3/\text{Co}$  powders. *J. Mater. Process. Tech.* **2008**, *202*, 457–463. [[CrossRef](#)]
9. Ma, J.; He, Y.D.; Wang, D.R.; Li, Z.W.; Gao, W. Oxidation of two-phase Cu–50 Cr alloy at low oxygen pressure. *Mater. Sci. Eng. A* **2006**, *434*, 141–146. [[CrossRef](#)]
10. Ma, J.; He, Y.D.; Wang, D.R.; Gao, W. The effects of pre-oxidation and thin  $\text{Y}_2\text{O}_3$  coating on the selective oxidation of Cr18–Ni9–Ti steel. *Mater. Lett.* **2004**, *58*, 807–812. [[CrossRef](#)]

11. Ma, J.; He, Y.D.; Sun, B.D.; Wang, J. High temperature corrosion behaviour of microcrystalline aluminide coating on Q235 steel. *Corros. Eng. Sci. Technol.* **2009**, *44*, 157–160. [[CrossRef](#)]
12. Kuprin, A.S.; Belous, V.A.; Voyevodin, V.N.; Bryk, V.V.; Vasilenko, R.L.; Ovcharenko, V.D.; Reshetnyak, E.N.; Tolmachova, G.N.; V'yugov, P.N. Vacuum-arc chromium-based coatings for protection of zirconium alloys from the high-temperature oxidation in air. *J. Nucl. Mater.* **2015**, *465*, 400–406. [[CrossRef](#)]
13. Chen, M.H.; Li, W.B.; Shen, M.L.; Zhu, S.L.; Wang, F.H. Glass coatings on stainless steels for high-temperature oxidation protection, Mechanisms. *Corros. Sci.* **2014**, *82*, 316–327. [[CrossRef](#)]
14. Zarchi, H.R.K.; Soltanieh, M.; Aboutalebi, M.R.; Guo, X. Thermodynamic study on pack aluminizing systems of pure titanium and nickel. *Trans. Nonferr. Metal. Soc.* **2013**, *23*, 1838–1846. [[CrossRef](#)]
15. Kawaura, H.; Kawahara, H.; Nishino, K.; Saito, T. New surface treatment using shot blast for improving oxidation resistance of TiAl-base alloys. *Mater. Sci. Eng. A* **2002**, *329*, 589–595. [[CrossRef](#)]
16. Wang, C.J.; Chen, S.M. The high-temperature oxidation behavior of hot-dipping Al–Si coating on low carbon steel. *Surf. Coat. Technol.* **2006**, *200*, 6601–6605. [[CrossRef](#)]
17. Liu, S.; Liu, Z.; Wang, Y.; Tang, J. A comparative study on the high-temperature corrosion of TP347H stainless steel, C22 alloy and laser-cladding C22 coating in molten chloride salts. *Corros. Sci.* **2014**, *83*, 396–408. [[CrossRef](#)]
18. Lehmusto, J.; Yrjas, P.; Hupa, L. Pre-oxidation as a means to increase corrosion resistance of commercial superheater steels. *Oxid. Met.* **2019**, *91*, 311–326. [[CrossRef](#)]
19. Yu, J.; Ji, G.; Liu, Q.; Zhang, J.B.; Shi, Z.M. Effect of sol-gel ZrO<sub>2</sub> films on corrosion behavior of the 304 stainless steel in coal-gases environment at high-temperature. *Surf. Coat. Technol.* **2017**, *331*, 21–26. [[CrossRef](#)]
20. Gestel, T.V.; Sebold, D.; Hauler, F.; Meulenberg, W.A.; Buchkremer, H.P. Potentialities of microporous membranes for H<sub>2</sub>/CO<sub>2</sub> separation in future fossil fuel power plants, evaluation of SiO<sub>2</sub>, ZrO<sub>2</sub>, Y<sub>2</sub>O<sub>3</sub>–ZrO<sub>2</sub> and TiO<sub>2</sub>–ZrO<sub>2</sub> sol-gel membranes. *J. Membr. Sci.* **2010**, *359*, 64–79. [[CrossRef](#)]
21. Cividanes, L.S.; Campos, T.M.B.; Rodrigues, L.A.; Brunelli, D.D.; Thim, G.P. Review of mullite synthesis routes by sol-gel method. *J. Sol. Gel. Sci. Technol.* **2010**, *55*, 111–125. [[CrossRef](#)]
22. Girolamo, D.G.; Blasi, C.; Pilloni, L.; Schioppa, M. Microstructural and thermal properties of plasma sprayed mullite coatings. *Ceram. Int.* **2010**, *36*, 1389–1395. [[CrossRef](#)]
23. Schneider, H.; Schreuer, J.; Hildmann, B. Structure and properties of mullite—A review. *J. Eur. Ceram. Soc.* **2008**, *28*, 329–344. [[CrossRef](#)]
24. Schneider, H.; Fischer, R.X.; Schreuer, J. Mullite: Crystal structure and related properties. *J. Am. Ceram. Soc.* **2015**, *98*, 2948–2967. [[CrossRef](#)]
25. Murshed, M.M.; Šehović, M.; Fischer, M.; Senyshyn, A.; Schneyder, H.; Gesing, T.M. Thermal behavior of mullite between 4K and 1320K. *J. Am. Ceram. Soc.* **2017**, *100*, 5259–5273. [[CrossRef](#)]
26. Zagorka, A.; Anja, T.; Ljubiša, A.; Ljubica, P.; Marko, P. Synthesizing a new type of mullite lining. *Mater. Technol.* **2013**, *47*, 777–780.
27. Lu, Z.L.; Tian, G.Q.; Wan, W.J.; Miao, K.; Li, D.C. Effect of in situ synthesised mullite whiskers on the high-temperature strength of Al<sub>2</sub>O<sub>3</sub>-based ceramic moulds for casting hollow turbine blades. *Ceram. Int.* **2016**, *42*, 18851–18858. [[CrossRef](#)]
28. Luz, A.P.; Neto, A.S.; Santos, T., Jr.; Medeiros, J.; Pandolfelli, V.C. Mullite-based refractory castable engineering for the petrochemical industry. *Ceram. Int.* **2013**, *39*, 9063–9070. [[CrossRef](#)]
29. Ueno, S.; Ohji, T.; Lin, H.T. Corrosion and recession of mullite in water vapor environment. *J. Eur. Ceram. Soc.* **2008**, *28*, 431–435. [[CrossRef](#)]
30. Zhou, L.; Fu, Q.G.; Huo, C.X.; Tong, M.D.; Liu, X.S.; Hu, D. Mullite whisker -mullite/yttrium aluminosilicate oxidation protective coatings for SiC coated C/C composites. *Ceram. Int.* **2019**, *45*, 24022–24030. [[CrossRef](#)]
31. Chen, P.J.; Xiao, P.; Li, Z.; Li, Y.; Li, J.W. Oxidation properties of tri-layer ytterbium-disilicate/mullite/silicon-carbide environment barrier coatings for C<sub>f</sub>/SiC composites. *Surf. Coat. Technol.* **2020**, *402*, 126329. [[CrossRef](#)]
32. Wen, Z.L.; Xiao, P.; Li, Z.; Hong, W.; Luo, H.; Yu, X.Y.; Li, Y.; Chen, W.B. Microstructure and oxidation behavior of sol-gel mullite coating on SiC-coated carbon/carbon composites. *J. Eur. Ceram. Soc.* **2015**, *35*, 3789–3796.
33. Ma, H.; Li, Y.F. Influence of sol-gel method on preparing mullite coating on stainless steel. *Bull. Chin. Ceram. Soc.* **2010**, *29*, 956–970.
34. Shen, J.Y. Properties and application of synthetic mullite refractories. *J. Bull. Chin. Ceram. Soc.* **1993**, *12*, 34–36.
35. Zhang, H.; Zhang, T.; Shao, Y.Q.; Tang, D.; Xia, P.; Ye, D.W. Comparison of high temperature protection effect of different coatings on 304 stainless steel. *J. Heat. Treat. Met.* **2012**, *37*, 96–101.
36. An, L.; Ma, Q.; Jia, J.G.; Li, P. Preparation of silicide layer on AISI 304 surface and its cyclic oxidation performance at 900 °C. *J. Hot Work. Technol.* **2011**, *40*, 137–140.
37. Wagner, R.C. Theoretical analysis of the diffusion processes determining the oxidation rate of alloys. *J. Electrochem. Soc.* **1952**, *10*, 369–380. [[CrossRef](#)]